Supporting Information

One-step Ethylene Purification from a Seven-component Cracking Gas Mixture with Sorbent-sorbate Induced-Fit

Xiaowan Peng[1†], Li Zhao[1,2†], Yun-Lei Peng[1,2,3,4*], Chenghua Deng[5], Yassin Hjiej Andaloussi[5], Huiyuan Pan[1], Yong-Jun Tian[1,2], Jin-Sheng Zou[1,2], Rajamani Krishna[6], Bei Liu[1], Chun Deng[1], Peng Xiao[1], Changyu Sun[1], Michael J. Zaworotko[5], Guangjin Chen[1*], Zhenjie Zhang[7*]

[1]State Key Laboratory of Heavy Oil Processing, China University of Petroleum, Beijing 102249, [2]Department of Applied Chemistry, College of Science, China University of Petroleum, Beijing 102249, [3]Basic Research Center for Energy, Interdisciplinary, College of Science, China University of Petroleum, Beijing 102249, [4]Beijing Key Laboratory of Optical Detection Technology for Oil and Gas, College of Science, China University of Petroleum, Beijing 102249, [5]Department of Chemical Sciences, Bernal Institute, University of Limerick, Limerick V94 T9PX, [6]Van't Hoff Institute for Molecular Sciences, University of Amsterdam, 1098 XH Amsterdam, [7]College of Chemistry, Nankai University, Tianjin, 300071

*Corresponding authors: *ylpeng@cup.edu.cn; zhangzhenjie@nankai.edu.cn; gjchen@cup.edu.cn*;

† X. Peng and L. Zhao contributed equally to this work.

Supplementary Text

Chemicals

All reagents and solvents were commercially purchased and used without further purification. Basic zinc carbonate ($3Zn(OH)_2{\cdot}2ZnCO_3$, 99%, Energy Chemical), Oxalate ($H_2C_2O_4$, 99.7%, Leyan), 1,2,4-triazole ($C_2H_3N_3$, 99.5%, Heowns), Ethanol (C_2H_5OH, anhydrous, 99.5%, Energy Chemical, Methyl cellulose ($C_{20}H_{38}O_{11}$, 99%, Bore), C_2H_4 (99.99%), C_2H_6 (99.999%), C_2H_2 (99%), C_2H_4 (99.99%), CO_2 (99.99%), C_3H_4 (99.999%), C_3H_6 (99.999%), C_3H_8 (99.999%), He (99.9999%), C_2H_6/C_2H_4 (50/50, v/v), $C_2H_2/C_2H_4/C_2H_6$ (33:33:33, v/v/v), $C_2H_2/C_2H_4/C_2H_6/CO_2$ (25:25:25, v/v/v/v), $CO_2/C_2H_2/C_2H_4/C_2H_6/C_3H_4/C_3H_6/C_3H_8$ (0.3/0.6/62/10/0.6/26/0.5, v/v/v/v/v/v/v) were purchased from Beijing Air Products BAIF Gases Industry Co., Ltd.

Preparation of of single crystal of CALF-20 and gas-loaded CALF-20

Single crystal of CALF-20 was synthesized at a milligram scale. The basic zinc carbonate (100 mg, $3Zn(OH)_2{\cdot}2ZnCO_3$), oxalate (100 mg, $H_2C_2O_4$) and 1,2,4-triazole (390 mg, $C_2H_3N_3$) was added in 8 mL water and 2 mL ethanol. After an hour of stirring, the mixtures were placed in a Teflon-lined autoclave and heated at 453 K for 48 h. After that, the products were naturally cooled to room temperature from 453 K, and the crystal was filtered from the growth solution and carefully washed with ethanol and water.

A single crystal of CALF-20 was selected and put into a capillary glass tube with inner diameter of 0.2 mm. This crystal was evacuated at 373 K for 12 h, and the capillary glass tube was filled by pure gas up to 1 bar and then sealed to obtain gas-loaded or gas-loaded CALF-20 crystal.

Preparation of CALF-20 powder at pilot-scale

The CALF-20 is synthesized on a 15 kg scale in a 200 L reaction vessel using a much greener modified method than previously reported [1,2]. The vessel was equipped with a heating coil, the working temperature is 293~353 K, and its maximum working pressure is 1 MPa. Typically, 10 kg of $3Zn(OH)_2{\cdot}2ZnCO_3$ was dissolved in the mixture of 20 L ethanol and 80 L of deionized water, and the mixtures were added into the reaction vessel through the material feeding port. Then, 4 kg of oxalate and 7 kg of 1,2,4-triazole were separately dissolved into 30 L of deionized water in two 60 L plastic beakers. The solutions were stirred for 40 min, and then add the solutions slowly to the reactor. The reaction mixture was heated to 333 K and maintained for 10 h. During the reaction, the spinner was stirred at 150 rpm. After the reaction, the mixtures were cooled down to

room temperature, and the CALF-20 product can be found as a white precipitate at the bottom of the vessel. The product was collected by filtration and washed with water. The white solids were transferred to aluminum foil pans, and placed in an oven at 373 K for 24 h. The overall yield of CALF-20 is about 85%.

Molding process for structured CALF-20

For further breakthrough experiments, powdered CALF-20 was structured using methyl cellulose as a binder. 3 g of methyl cellulose was added to a beaker. Then, 30 g of powder CALF-20 was added and the mixture was stirred for 5 h at room temperature. The resulting mixture was blended with 10 g of deionized water to form sand-granular pellets. Then, the mixture was extruded into a double screw extruder to produce a structured CALF-20. The particle density of the structured CALF-20 sample was measured at 690 kg/m^3, and the particle size was about 1.0-2.0 mm. After extruding, the average particle strength is measured as 54.21 N/cm.

Breakthrough experiments

The breakthrough tests were investigated on the home-built gas breakthrough apparatus at 298 K and 1 bar using a glass tube (6 mm inner diameter ×300 mm) or a stainless steel column (3.3 cm inner diameter × 13 cm). For the breakthrough tests for 3g CALF-20 powders, the materials were activated at 373 K for 14 h with He purging (20 mL/min). As the temperature cooled down to room temperature, stop the He purging and the feed gases (C_2H_6/C_2H_4, 50/50, $C_2H_2/C_2H_4/C_2H_6$, 33/33/33; v/v/v, $CO_2/C_2H_2/C_2H_6/C_2H_4$ (25:25:25:25, v/v/v/v) were introduced to the adsorber with a flowrate of 2 mL/min. The gas at the exit was examined via a mass spectrometer (HIDEN HPR-20 EGA). When the dynamic adsorption equilibrium was reached, the adsorber was then purged with He (20 mL/min) at 353 K for 2 h or by vacuuming for 30 min at 353 K for regeneration.

For the breakthrough tests for 30 g structured samples, we used stainless steel column (3.3 cm inner diameter × 13cm). Firstly, the samples were activated using a purge with He gas (65 mL/min) at 373 K for 16 h. The gas mixture ($CO_2/C_2H_2/C_2H_4/C_2H_6/C_3H_4/C_3H_6/C_3H_8$ (0.3/0.6/62/10/0.6/26/0.5)) then flowed through the adsorber with a flowrate of 12 mL/min. The gas eluted from the exit was detected by the mass spectrometer. After the breakthrough test, the adsorber was regenerated by vacuuming for 5 h at 373 K.

Note that the in order to avoid overlapping peaks of hydrocarbon gases, soft ionization techniques of mass spectrometry are used. 74% humidity is controlled by a hygrometer.

The C_2H_4 productivity (q) was obtained by integrating the breakthrough curve area from t_1 to t_2 in which the C_2H_4 purity is over 99.95%.

$$q = \frac{\int_{t_1}^{t_2} \frac{C}{C_0}(t)dt}{m} \cdot r \cdot z_i \tag{1}$$

where t (min) is time, m is the mass of the samples used in the breakthrough experiments, f is C/C_0, r is the flow rate (mL/min), z_i is the mole fraction of component.

Gas selectivity prediction via IAST

The adsorption isotherms for pure C_2H_2, C_2H_4, and C_2H_6 were fitted with excellent accuracy using a single-site Langmuir-Freundlich model.

$$n = q_{sat} \frac{bp^C}{1+bp^C} \tag{2}$$

For CO_2, C_3H_4, C_3H_6 and C_3H_8, the isotherms were fitted by using a dual-site Langmuir-Freundlich model where we distinguish two distinct adsorption sites:

$$n = q_{sat,A} \frac{b_A p^{C_A}}{1+b_A p^{C_A}} + q_{sat,B} \frac{b_B p^{C_B}}{1+b_B p^{C_B}} \tag{3}$$

Here, p is the pressure of the bulk gas at equilibrium with the adsorbed phase (kPa), n is the adsorbed amount per mass of adsorbent (mmol/g), q_{sat} is the saturation capacity (mmol/g), b is the affinity coefficient (kPa^{-1}).

The selectivity of the preferential adsorption of component 1 over component 2 in a mixture containing 1 and 2 can be formally defined as:

$$S_{i/j} = \frac{x_i \cdot y_j}{x_j \cdot y_i} \tag{4}$$

In the above equation, x_i and y_i (x_j and y_j) are the molar fractions of component i (component j) in the adsorbed and bulk phases, respectively. We calculated the values of x_i and x_j using the ideal adsorbed solution theory (IAST) of Myers and Prausnitz.

Isosteric heat of adsorption calculation

The adsorption heat calculations are based on the Clausius-Clapeyron equation[3]. The specific methods are as follows:

$$Q_{st} = -RT^2 \left(\frac{\partial \ln p}{\partial T}\right)_q \tag{5}$$

where Q_{st} (kJ/mol) is the coverage-dependent enthalpy of adsorption and R is the universal gas constant, T (K) is the temperature, P (bar) is the pressure, and q (mmol/g) is the adsorbed amount.

Theoretical calculation details

Simulations in CALF-20 were performed on the single X-ray crystallographic structure as published in reference (CCDC 2084733).[1] All the calculations were performed in the Materials Studio 7.0. Grand canonical Monte Carlo (GCMC) simulations of CALF-20 were conducted using the located module. We performed the structural optimization by the $Dmol^3$ module. The CALF-20 framework is considered rigid during the simulation. Partial charges for atoms of CALF-20 were obtained by using QEq method and QEq_neutral1.0 parameter. The calculations were performed using the locate task, Metropolis method in Sorption module and the universal force field (UFF) at 298 K. The partial charges for the atoms of gases were obtained by using QEq method. The binding energy between gas molecules and framework were calculated via the Coulomb and Lennard-Jones 6-12 (LJ) potentials. For the LJ potential, the cutoff radius was selected as 8.9 Å and the long-range electrostatic interactions were coped with the Atom-based summation method. The equilibration steps and the loading steps were 1×10^6, the production steps were 5×10^7. The locate task simulated the beneficial adsorption sites with a single guest molecule. The binding energy between the guest and framework was computed by equation 3 and the molecular electrostatic potential-based (ESP) charges were calculated using the $DMOL^3$ module.

$$\Delta E = E_{(MOF)} + E_{(gas)} - E_{(MOF+gas)} \quad (6)$$

Supplementary Figures

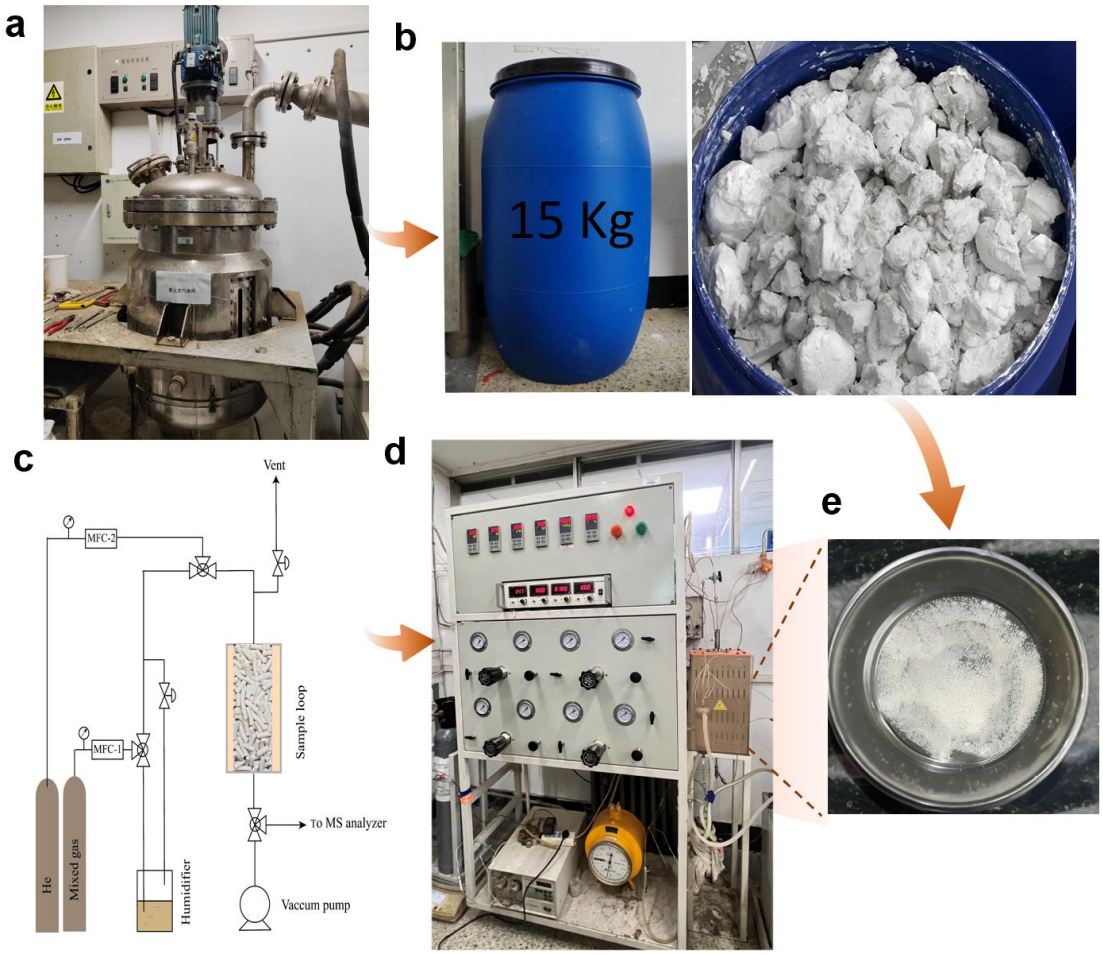

Figure S1. Large-scale preparation of CALF-20 and application. (a) A 15-kg-scale synthesis of CALF-20 in a 200 L reaction vessel; (b) Picture of large preparation of CALF-20 sample; The schematic (c) and test rig picture (d) of dynamic column breakthrough apparatus; (e) Structured CALF-20 (Particle size: 1.0-2.0 mm).

Figure S2. The pictures of the large preparation of the dry CALF-20 sample.

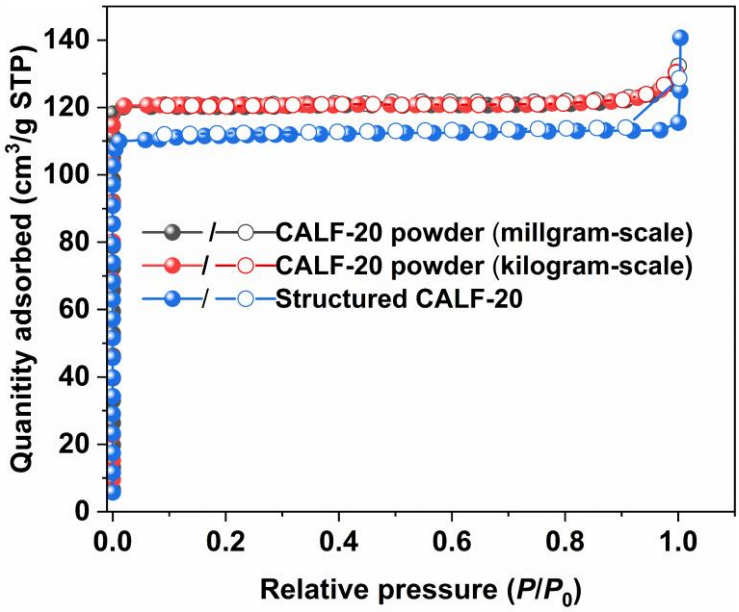

Figure S3. N_2 adsorption-desorption isotherm at 77 K. Milligram-scale (BET surface area 516 m^2/g); Kilogram-scale (BET surface area 501 m^2/g); Structured samples (BET surface area 490 m^2/g). *P*, nitrogen pressure; P_0 = 1 atm; STP, standard temperature and pressure.

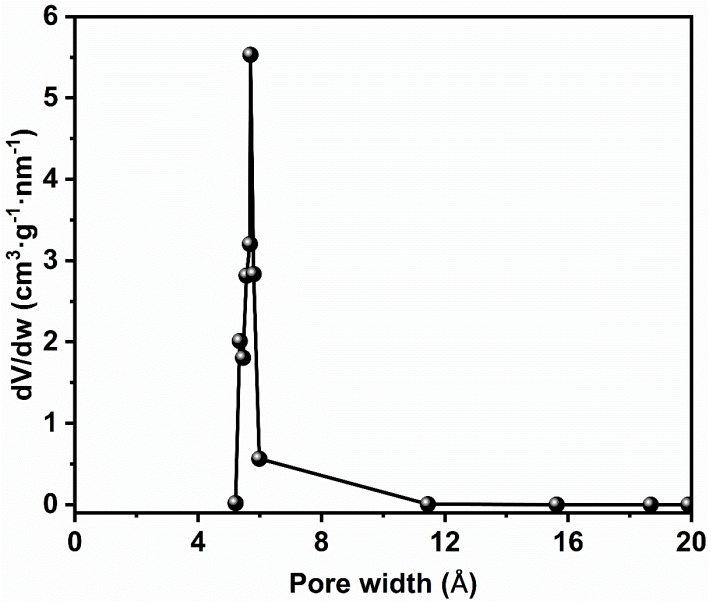

Figure S4. Pore size distribution profile of CALF-20 samples produced on milligram scale calculated by the Horvath-Kawazoe model (pore geometry: silt).

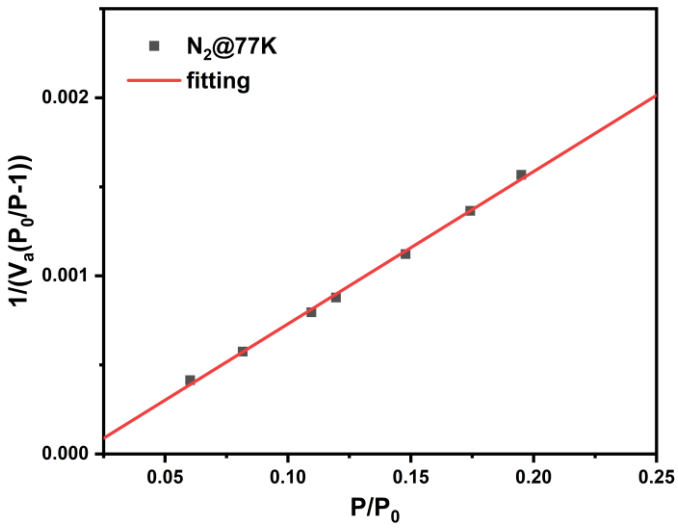

Figure S5. Calculation of BET surface area for CALF-20 obtained from N_2 adsorption isotherm at 77 K.

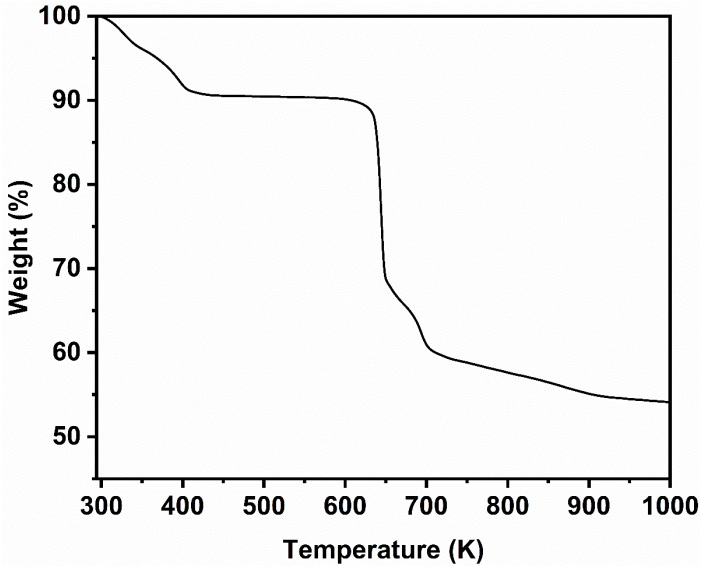

Figure S6. The TG analysis of CALF-20 performed under N_2 atmosphere.

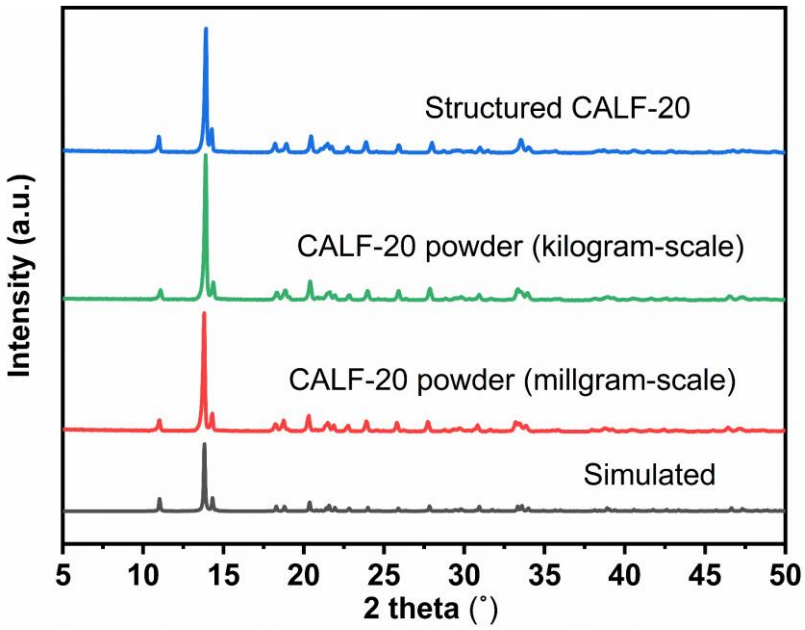

Figure S7. The PXRD patterns of CALF-20 powders produced at varying production scales and structured samples.

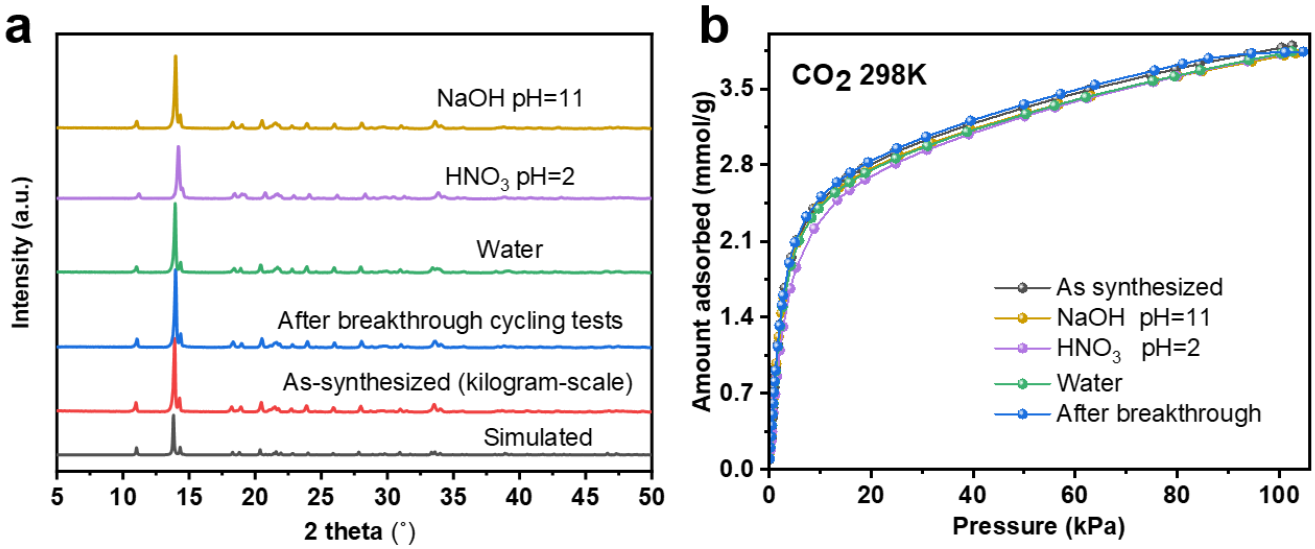

Figure S8. The PXRD patterns and CO_2 adsorption isotherms after various treatments.

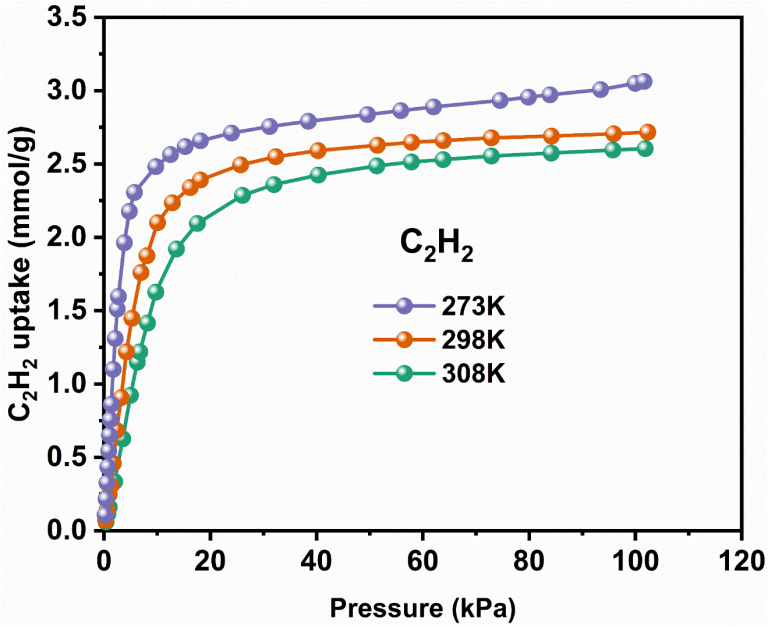

Figure S9. C_2H_2 adsorption isotherms on CALF-20 recorded at 273, 298 and 308 K.

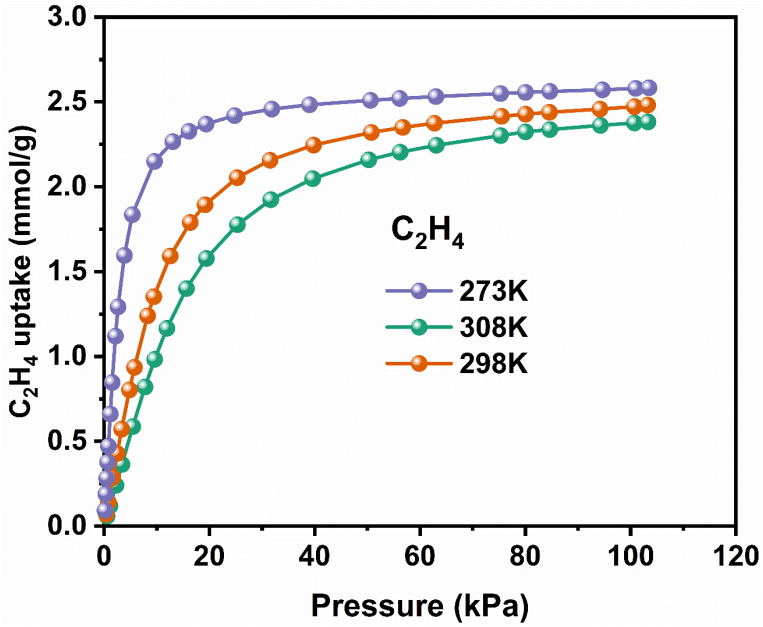

Figure S10. C_2H_4 adsorption isotherms on CALF-20 recorded at 273, 298 and 308 K.

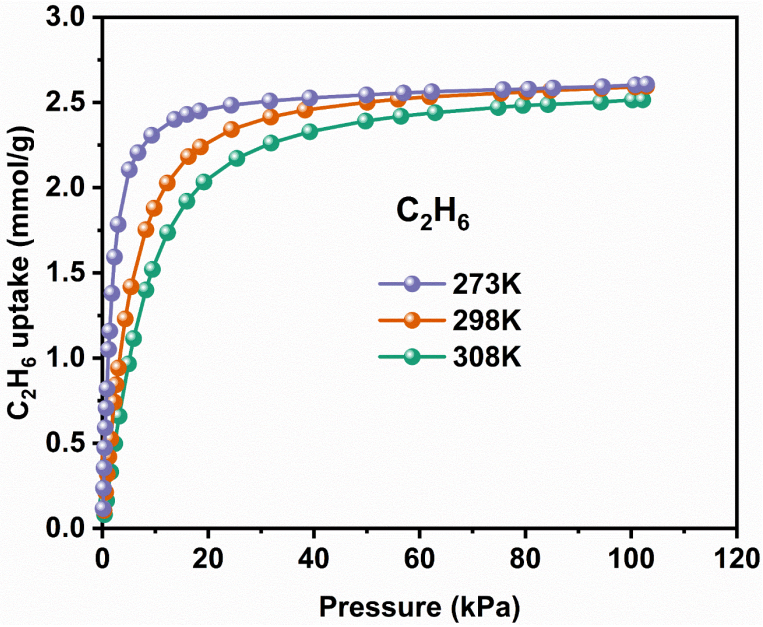

Figure S11. C_2H_6 adsorption isotherms on CALF-20 recorded at 273, 298 and 308 K.

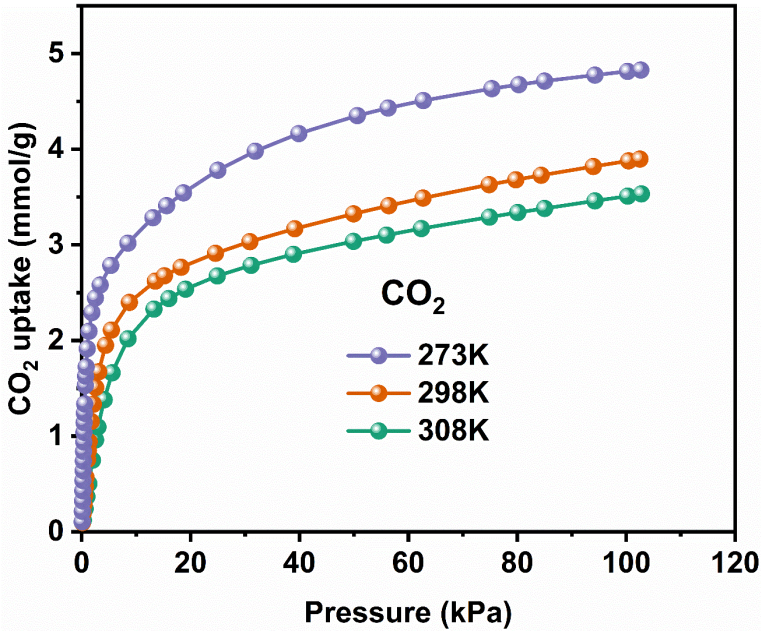

Figure S12. CO_2 adsorption isotherms on CALF-20 recorded at 273, 298 and 308 K.

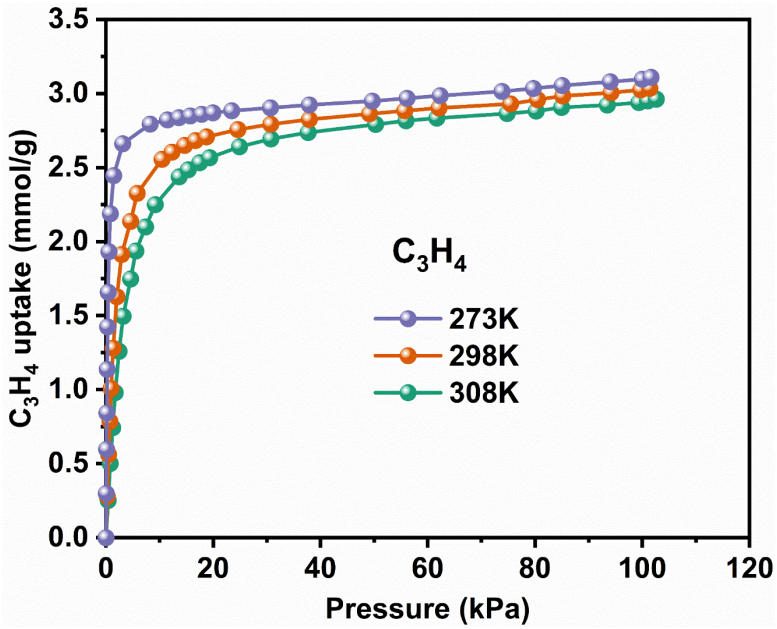

Figure S13. C_3H_4 adsorption isotherms on CALF-20 recorded at 273, 298 and 308 K.

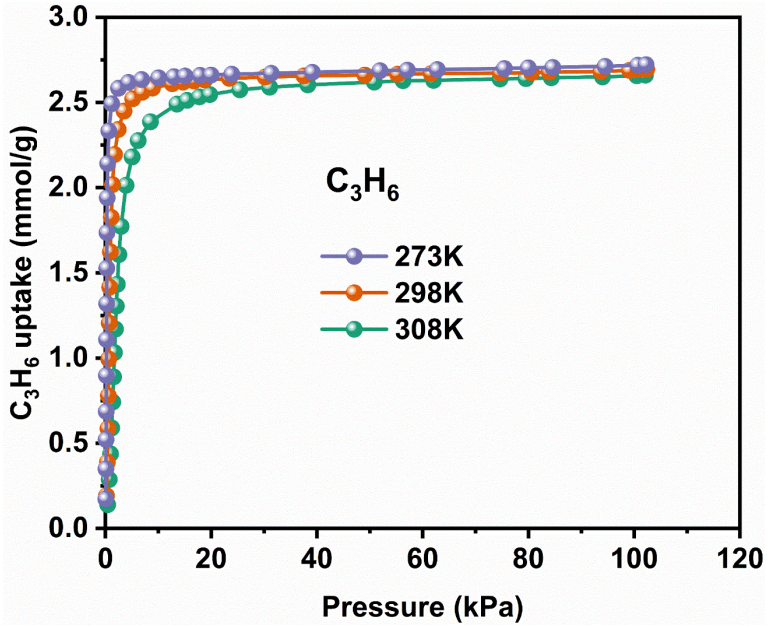

Figure S14. C_3H_6 adsorption isotherms on CALF-20 recorded at 273, 298 and 308 K.

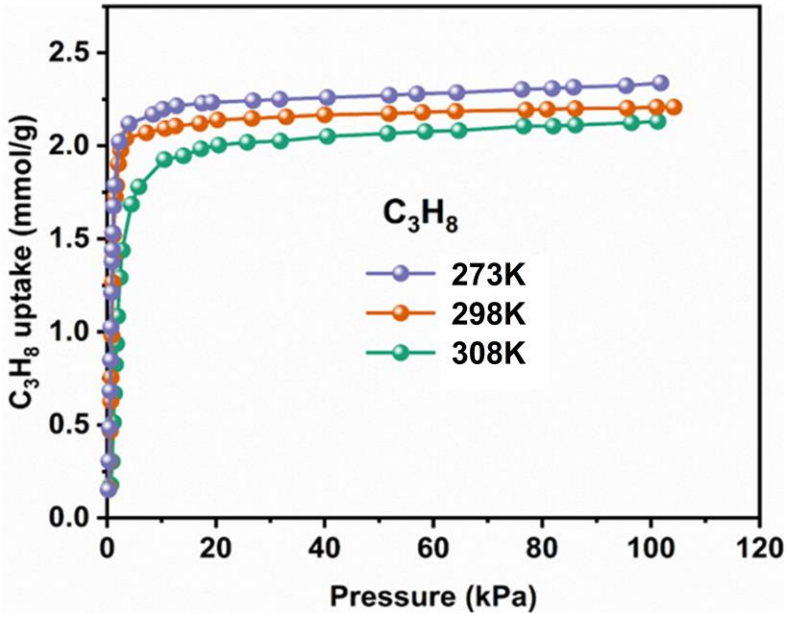

Figure S15. C_3H_8 adsorption isotherms on CALF-20 recorded at 273, 298 and 308 K.

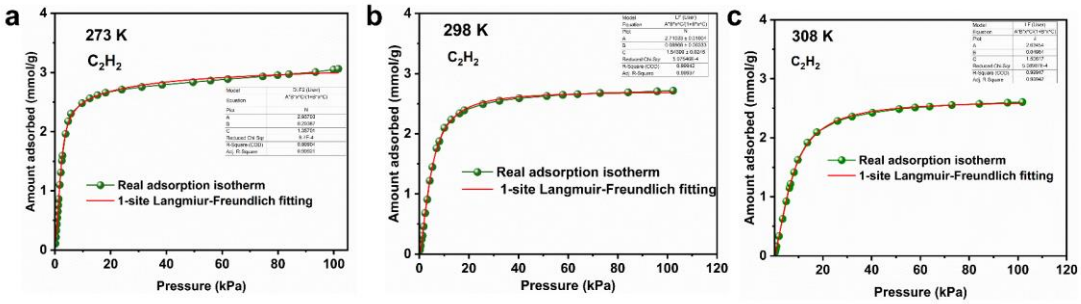

Figure S16. Single-site Langmuir-Freundlich model fits of C_2H_2 adsorption isotherms at 273 K(a), 298 K(b) and 308 K(c) in CALF-20.

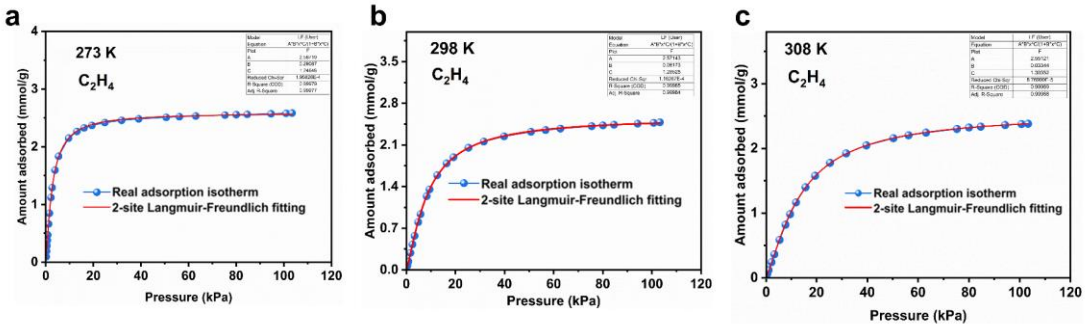

Figure S17. Single-site Langmuir-Freundlich model fits of C_2H_4 adsorption isotherms at 273 K(a), 298 K(b) and 308 K(c) in CALF-20.

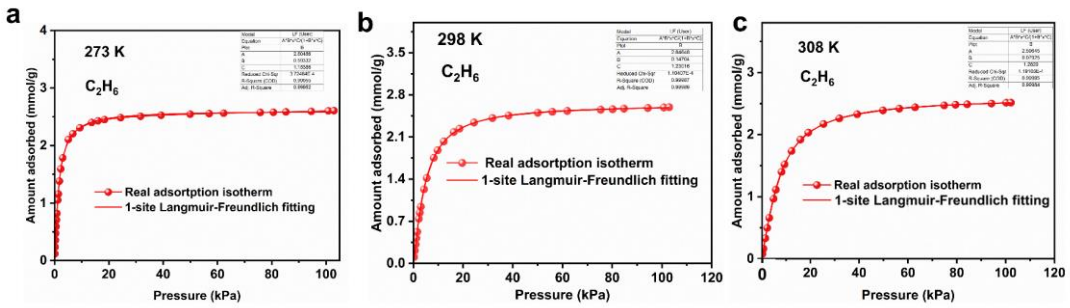

Figure S18. Single-site Langmuir-Freundlich model fits of C_2H_6 adsorption isotherms at 273 K(a), 298 K(b) and 308 K(c) in CALF-20.

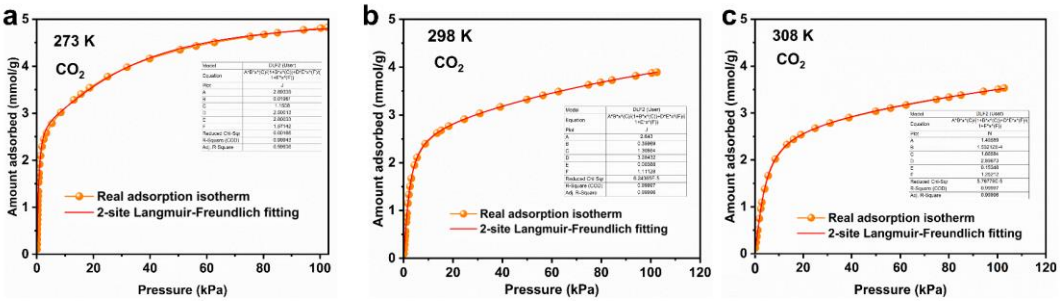

Figure S19. Dual-site Langmuir-Freundlich model fits of CO_2 adsorption isotherms at 273 K(a), 298 K(b) and 308 K(c) in CALF-20.

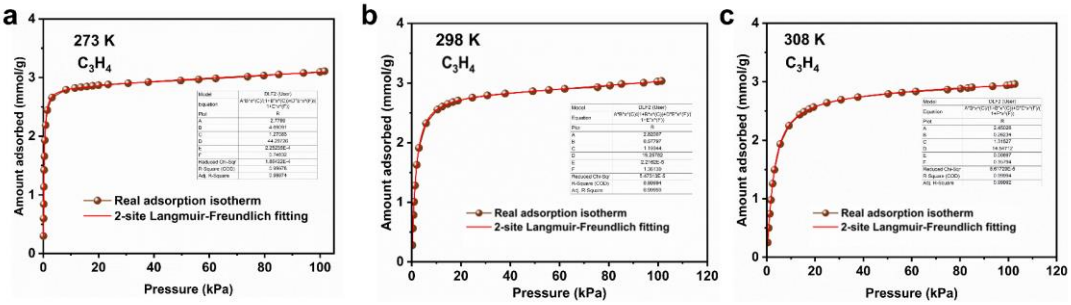

Figure S20. Dual-site Langmuir-Freundlich model fits of C_3H_4 adsorption isotherms at 273 K(a), 298 K(b) and 308 K(c) in CALF-20.

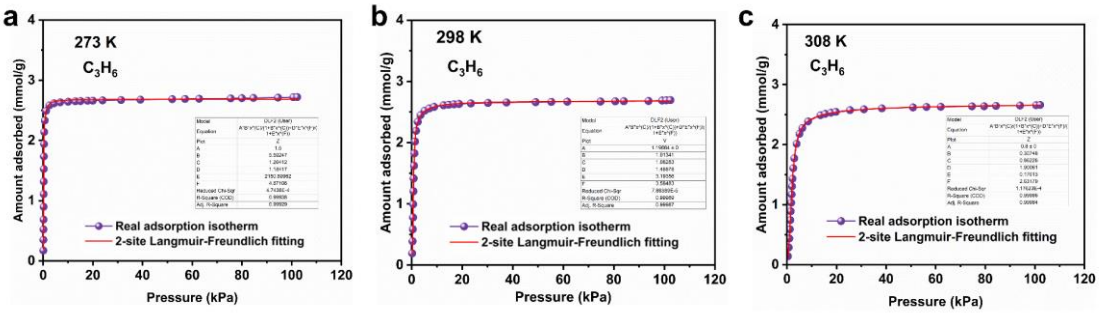

Figure S21. Dual-site Langmuir-Freundlich model fits of C_3H_6 adsorption isotherms at 273 K(a), 298 K(b) and 308 K(c) in CALF-20.

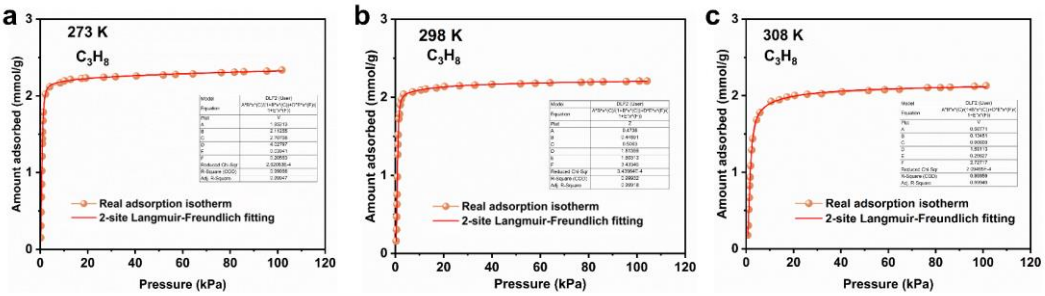

Figure S22. Dual-site Langmuir-Freundlich model fits of C_3H_8 adsorption isotherms at 273 K(a), 298 K(b) and 308 K(c) in CALF-20.

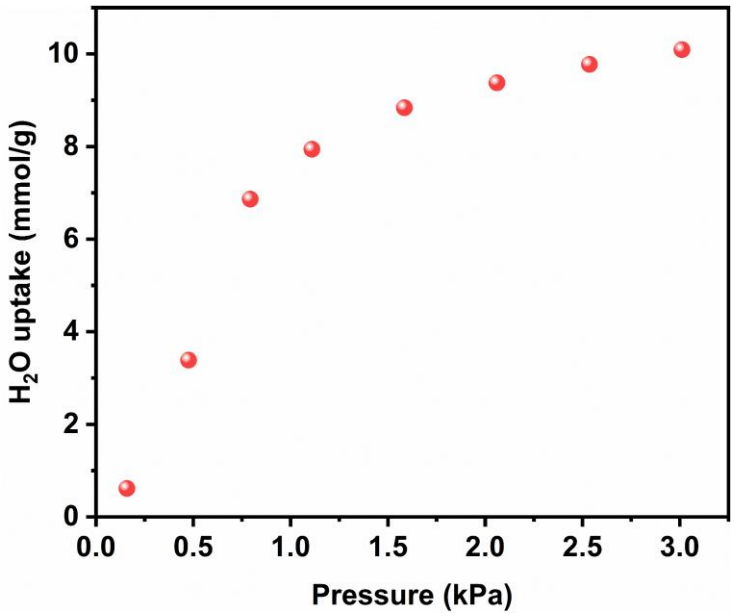

Figure S23. H_2O adsorption isotherm for CALF-20 at 298 K.

Supplementary Tables

Table S1. Crystal data of C_2H_4@CALF-20.

Identification code	C_2H_4@CALF-20
Empirical formula	$C_8H_8N_6O_4Zn_2$
Formula weight	382.94
Temperature/K	100.00(10)
Crystal system	monoclinic
Space group	$P2_1/c$
a/Å	8.9703(5)
b/Å	9.7335(4)
c/Å	9.4279(5)
α/°	90
β/°	116.627(7)
γ/°	90
Volume/Å^3	735.87(8)
Z	2
ρ_{calc}g/cm^3	1.728
μ/mm^{-1}	4.229
F(000)	380.0
Crystal size/mm^3	0.104 × 0.054 × 0.051
Radiation	Cu Kα (λ = 1.54184)
2Θ range for data collection/°	11.034 to 148.084
Index ranges	-10 ≤ h ≤ 10, -11 ≤ k ≤ 11, -11 ≤ l ≤ 10
Reflections collected	4561
Independent reflections	1405 [R_{int} = 0.0253, R_{sigma} = 0.0281]
Data/restraints/parameters	1405/9/99
Goodness-of-fit on F^2	1.103
Final R indexes [I>=2σ (I)]	R_1 = 0.0311, wR_2 = 0.0818
Final R indexes [all data]	R_1 = 0.0334, wR_2 = 0.0829
Largest diff. peak/hole / e Å^{-3}	0.68/-0.76

Table S2. Crystal data of C_2H_6@CALF-20.

Identification code	C_2H_6@CALF-20
Empirical formula	$C_8H_{10}N_6O_4Zn_2$
Formula weight	384.96
Temperature/K	99.99(10)
Crystal system	monoclinic
Space group	$P2_1/c$
a/Å	8.9920(3)
b/Å	9.7013(2)
c/Å	9.4416(3)
α/°	90
β/°	116.554(4)
γ/°	90
Volume/Å^3	736.75(4)
Z	2
ρ_{calc}g/cm^3	1.735
μ/mm^{-1}	4.224
F(000)	384.0
Crystal size/mm^3	0.105 × 0.057 × 0.048
Radiation	Cu Kα (λ = 1.54184)
2Θ range for data collection/°	11 to 146.838
Index ranges	$-10 \leq h \leq 10$, $-9 \leq k \leq 11$, $-11 \leq l \leq 10$
Reflections collected	4035
Independent reflections	1393 [R_{int} = 0.0164, R_{sigma} = 0.0158]
Data/restraints/parameters	1393/0/92
Goodness-of-fit on F^2	1.090
Final R indexes [I>=2σ (I)]	R_1 = 0.0244, wR_2 = 0.0657
Final R indexes [all data]	R_1 = 0.0251, wR_2 = 0.0662
Largest diff. peak/hole / e Å^{-3}	0.65/-0.49

Table S3. Crystal data of C_2H_2@CALF-20.

Identification code	C_2H_2@CALF-20
Empirical formula	$C_8H_6N_6O_4Zn_2$
Formula weight	380.93
Temperature/K	99.99(10)
Crystal system	monoclinic
Space group	*P2₁/c*
a/Å	8.9575(6)
b/Å	9.5520(5)
c/Å	9.6601(6)
α/°	90
β/°	115.487(7)
γ/°	90
Volume/Å^3	746.10(9)
Z	2
ρ_{calc}g/cm^3	1.696
μ/mm^{-1}	4.170
F(000)	376.0
Crystal size/mm^3	0.148 × 0.073 × 0.058
Radiation	Cu Kα (λ = 1.54184)
2Θ range for data collection/°	10.942 to 148
Index ranges	-10 ≤ h ≤ 10, -11 ≤ k ≤ 7, -11 ≤ l ≤ 12
Reflections collected	3978
Independent reflections	1393 [R_{int} = 0.0168, R_{sigma} = 0.0144]
Data/restraints/parameters	1393/12/100
Goodness-of-fit on F^2	1.117
Final R indexes [I>=2σ (I)]	R_1 = 0.0388, wR_2 = 0.1091
Final R indexes [all data]	R_1 = 0.0392, wR_2 = 0.1094
Largest diff. peak/hole / e Å^{-3}	0.76/-1.07

Table S4. Crystal data of CO_2@CALF-20.

Identification code	CO_2@CALF-20
Empirical formula	$C_7H_4N_6O_6Zn_2$
Formula weight	398.90
Temperature/K	100.00(10)
Crystal system	monoclinic
Space group	*P21/c*
a/Å	8.9738(15)
b/Å	10.0326(12)
c/Å	9.1756(18)
α/°	90
β/°	118.57(2)
γ/°	90
Volume/Å^3	725.5(3)
Z	2
ρcalcg/cm^3	1.826
μ/mm^{-1}	4.431
F(000)	392.0
Crystal size/mm^3	0.086 × 0.048 × 0.039
Radiation	Cu Kα (λ = 1.54184)
2Θ range for data collection/°	11.228 to 156.846
Index ranges	$-10 \le h \le 8$, $-12 \le k \le 12$, $-10 \le l \le 11$
Reflections collected	6821
Independent reflections	1399 [R_{int} = 0.0706, R_{sigma} = 0.0385]
Data/restraints/parameters	1399/33/109
Goodness-of-fit on F^2	1.108
Final R indexes [I>=2σ (I)]	R_1 = 0.0839, wR_2 = 0.2366
Final R indexes [all data]	R_1 = 0.0948, wR_2 = 0.2579
Largest diff. peak/hole / e Å^{-3}	2.12/-1.61

Table S5. Crystal data of C_3H_4@CALF-20.

Identification code	C_3H_4@CALF-20
Empirical formula	$C_9H_8N_6O_4Zn_2$
Formula weight	394.95
Temperature/K	100.01(10)
Crystal system	monoclinic
Space group	$P2_1/c$
a/Å	8.9643(5)
b/Å	10.0872(4)
c/Å	9.1635(5)
α/°	90
β/°	118.696(8)
γ/°	90
Volume/Å^3	726.84(8)
Z	2
ρ_{calc}g/cm^3	1.805
μ/mm^{-1}	4.306
F(000)	392.0
Crystal size/mm^3	0.124 × 0.047 × 0.043
Radiation	Cu Kα (λ = 1.54184)
2Θ range for data collection/°	11.252 to 148.396
Index ranges	$-10 \leq h \leq 10$, $-12 \leq k \leq 12$, $-9 \leq l \leq 11$
Reflections collected	3432
Independent reflections	1391 [R_{int} = 0.0183, R_{sigma} = 0.0203]
Data/restraints/parameters	1391/20/110
Goodness-of-fit on F^2	1.129
Final R indexes [I>=2σ (I)]	R_1 = 0.0427, wR_2 = 0.1202
Final R indexes [all data]	R_1 = 0.0453, wR_2 = 0.1221
Largest diff. peak/hole / e Å^{-3}	0.68/-1.19

Table S6. Crystal data of C_3H_6@CALF-20.

Identification code	C_3H_6@CALF-20
Empirical formula	$C_9H_{10}N_6O_4Zn_2$
Formula weight	396.97
Temperature/K	100.00(10)
Crystal system	monoclinic
Space group	*P21/c*
a/Å	8.9392(2)
b/Å	9.43330(10)
c/Å	9.7633(2)
α/°	90
β/°	114.630(2)
γ/°	90
Volume/Å^3	748.40(3)
Z	2
ρcalcg/cm^3	1.762
μ/mm^{-1}	4.182
F(000)	396.0
Crystal size/mm^3	0.113 × 0.067 × 0.042
Radiation	Cu Kα (λ = 1.54184)
2Θ range for data collection/°	10.888 to 149.166
Index ranges	-11 ≤ h ≤ 10, -11 ≤ k ≤ 11, -11 ≤ l ≤ 11
Reflections collected	6681
Independent reflections	1465 [R_{int} = 0.0250, R_{sigma} = 0.0201]
Data/restraints/parameters	1465/2/110
Goodness-of-fit on F^2	1.066
Final R indexes [I>=2σ (I)]	R_1 = 0.0223, wR_2 = 0.0566
Final R indexes [all data]	R_1 = 0.0236, wR_2 = 0.0572
Largest diff. peak/hole / e Å^{-3}	0.35/-0.45

Table S7. Crystal data of C_3H_8@CALF-20.

Identification code	C_3H_8@CALF-20
Empirical formula	$C_9H_{12}N_6O_4Zn_2$
Formula weight	398.99
Temperature/K	169(30)
Crystal system	monoclinic
Space group	*P21/c*
a/Å	8.9617(9)
b/Å	9.8133(7)
c/Å	9.3937(9)
α/°	90
β/°	116.932(12)
γ/°	90
Volume/Å^3	736.52(13)
Z	2
ρcalcg/cm^3	1.799
μ/mm^{-1}	4.250
F(000)	400.0
Crystal size/mm^3	0.113 × 0.048 × 0.042
Radiation	Cu Kα (λ = 1.54184)
2Θ range for data collection/°	11.074 to 146.614
Index ranges	-10 ≤ h ≤ 10, -10 ≤ k ≤ 11, -11 ≤ l ≤ 11
Reflections collected	3002
Independent reflections	1356 [R_{int} = 0.0324, R_{sigma} = 0.0278]
Data/restraints/parameters	1356/22/111
Goodness-of-fit on F^2	1.145
Final R indexes [I>=2σ (I)]	R_1 = 0.0626, wR_2 = 0.1755
Final R indexes [all data]	R_1 = 0.0649, wR_2 = 0.1774
Largest diff. peak/hole / e Å^{-3}	1.34/-1.02

Table S8. Single-site Langmuir-Freundlich parameter fits for C2 hydrocarbon and Dual-site Langmuir-Freundlich parameter fits for CO_2, C_3H_4, C_3H_6, C_3H_8 on CALF-20 at 273 K, 298 K and 308 K. R^2 values are also provided.

Guest	Temperature (K)	Site A			Site B			R^2
		$q_{sat,A}$(mmol/g)	b_A/kPa^{-1}	c_A	$q_{sat,B}$(mmol/g)	b_B/kPa^{-1}	c_B	
C_2H_2	273	2.93703	0.29387	1.35701	-	-	-	0.9992
	298	2.71033	0.08868	1.54399				0.9994
	308	2.63454	0.04964	1.50617				0.9995
C_2H_4	273	2.58719	0.29087	1.24648	-	-	-	0.9994
	298	2.5714	0.06173	1.2853				0.9996
	308	2.5512	0.03344	1.3035				0.9999
C_2H_6	273	2.6474	0.5795	1.0975	-	-	-	0.9995
	298	2.6465	0.14704	1.23016				0.9993
	308	2.59645	0.07925	1.2829				0.9992
CO_2	273	2.89339	0.01961	1.15081	2.50	2.80033	1.5714	0.9994
	298	2.643	0.3597	1.30864	3.2843	0.00368	1.11128	0.9999
	308	1.49589	0.00015	1.86584	2.8967	0.15348	1.25	0.9999
C_3H_4	273	2.7799	4.69093	1.2708	44.2973	0.000225	0.74832	0.9997
	298	2.82007	0.57795	1.194	19.25782	2.2162E-5	1.36139	0.9994
	308	2.4503	0.26234	1.31527	14.5471	0.00697	0.35794	0.9999
C_3H_6	273	1.50	5.59281	1.26417	1.18416	2150.9	4.87106	0.9994
	298	1.19664	1.01376	1.08328	1.48865	3.19336	3.58457	0.9995
	308	0.8	0.30732	0.86316	1.90042	0.17026	2.63096	0.9998
C_3H_8	273	1.95213	2.11255	2.70758	4.028	0.03941	0.2055	0.9996
	298	1.81395	1.60313	3.4335	0.4738	0.4489	0.5063	0.9993
	308	1.59113	0.26627	2.7272	0.56771	0.13481	0.96669	0.9995

Table S9. Summary of benchmark MOF for one-step C_2H_4 purification from ternary mixture ($C_2H_2/C_2H_4/C_2H_6$) and quaternary mixture ($C_2H_2/C_2H_4/C_2H_6/CO_2$)

Adsorbents	$C_2H_6/C_2H_2/C_2H_4/CO_2$ Q_{st} (kJ/mol)	C_2H_6 uptake at 10 kPa (mmol g^{-1})	IAST selectivity (100 kPa)			Reference
			C_2H_6/C_2H_4 (10/90)	C_2H_2/C_2H_4 (1/99)	CO_2/C_2H_4 (1/1)	
CALF-20	**35.9/30.9/30.0/36.8**	**1.88**	**1.99**	**2.03**	**6.38**	**This work**
Zn-atz-oba	30.0/27.5/27.0/29.08	0.64	1.27 [a]	1.43 [b]	1.33	[4]
Zn-ATA	32.5/24.5/27.4	0.80	1.83	1.8		[5]
TJT-100	29.0/31.0/25.0	1.21	1.2	1.8		[6]
Azole-Th-1	28.6/--/26.1	0.85	1.44	1.09 [b]		[7]
NUM-9a	35.8/35.8/32.3	1.07	1.62	1.48		[8]
CuTiF6-TPPY	34.2/36.5/29.6	1.33	2.12	5.03		[9]
NPU-1	29.1/27.8/23.9	1.30	1.32 [a]	1.4 [b]		[10]
Zn(ad)(int)	33.3/34.7/29.0	1.83	2.40	1.61		[11]
[Zn(BDC)(H_2BPZ)]	31.8/28.7/23.2	1.96	2.20	1.6		[12]
ZJNU-7	29.7/34.1/29.3	1.38	1.56	1.77		[13]
ZJNU-115	28.2/29.2/27.7	1.07	1.56 [a]	2.05		[14]
UiO-67-$(NH_2)_2$	26.5/27.4/24.5	1.11	1.7 [a]	2.1		[15]
UiO-66-CF_3	24.32/24.27/22.18	0.46	1.9	1.4		[16]
UPC-612	22.39/23.94/16.94	0.45	1.07	1.08 [c]		[17]
UPC-613	31.8/30.4/28.5	0.65	1.5	1.4 [c]		[17]
UPC-66-a	15.6/17.6/17.8	0.50	1.65	1.05		[18]
BUT-151	31.06/36.81/23.95	1.08	1.26 [a]	1.61 [b]		[19]
LIFM-XYY-6	32.2/37.1/31.5	0.45	1.63	1.53 [b]		[20]
HIAM-210	31.2/34.3/22.7	0.79	2.0 [a]	2.0 [b]		[21]
HIAM-326	27.5/25/23.4	0.69	1.85	1.55		[22]
MOF-303	35.4/38.4/33.7	1.66	1.7 [a]	2.4		[23]

[a] C_2H_6/C_2H_4 = 50:50
[b] C_2H_2/C_2H_4 = 50:50
[c] C_2H_2/C_2H_4 = 10:90

Table S10. The raw materials cost of CALF-20

Materials	Reagents					CALF-20
	$3Zn(OH)_2{\cdot}2ZnCO_3$	Oxalate	1,2,4-triazole	ethanol	deionized water	
Price ($ /kg)	~5.5	~6.9	~8.1	~2.5	0.002	~12.7

Note: $3Zn(OH)_2{\cdot}2ZnCO_3$ (99%) and ethanol (99.5%) were purchased from Energy Chemical. Oxalate (99.7%) was purchased from Leyan. And 1,2,4-triazole (99.5%) was purchased from Heowns. The cost of equipment is not considered.

References

[1] J.-B. Lin, T. T. T. Nguyen, R. Vaidhyanathan, J. Burner, J. M. Taylor, H. Durekova, F. Akhtar, R. K. Mah, O. Ghaffari-Nik, S. Marx, N. Fylstra, S. S. Iremonger, K. W. Dawson, P. Sarkar, P. Hovington, A. Rajendran, T. K. Woo, G. K. H. Shimizu, *Science* **2021**, *374*, 1464-1469.

[2] G. Sheldrick, G. M. Sheldrick, G. M. Sheldrick, **1997**.

[3] S. Builes, S. I. Sandler, R. Xiong, *Langmuir* **2013**, *29*, 10416-10422.

[4] J.-W. Cao, S. Mukherjee, T. Pham, Y. Wang, T. Wang, T. Zhang, X. Jiang, H.-J. Tang, K. A. Forrest, B. Space, M. J. Zaworotko, K.-J. Chen, *Nature Communications* **2021**, *12*, 6507.

[5] Q. Ding, Z. Zhang, P. Zhang, C. Yu, C.-H. He, X. Cui, H. Xing, *Chemical Engineering Journal* **2022**, *450*, 138272.

[6] H.-G. Hao, Y.-F. Zhao, D.-M. Chen, J.-M. Yu, K. Tan, S. Ma, Y. Chabal, Z.-M. Zhang, J.-M. Dou, Z.-H. Xiao, G. Day, H.-C. Zhou, T.-B. Lu, *Angewandte Chemie International Edition* **2018**, *57*, 16067-16071.

[7] Z. Xu, X. Xiong, J. Xiong, R. Krishna, L. Li, Y. Fan, F. Luo, B. Chen, *Nature Communications* **2020**, *11*, 3163.

[8] S.-Q. Yang, F.-Z. Sun, P. Liu, L. Li, R. Krishna, Y.-H. Zhang, Q. Li, L. Zhou, T.-L. Hu, *ACS Applied Materials & Interfaces* **2021**, *13*, 962-969.

[9] P. Zhang, Y. Zhong, Y. Zhang, Z. Zhu, Y. Liu, Y. Su, J. Chen, S. Chen, Z. Zeng, H. Xing, S. Deng, J. Wang, *Science Advances*, *8*, eabn9231.

[10] B. Zhu, J.-W. Cao, S. Mukherjee, T. Pham, T. Zhang, T. Wang, X. Jiang, K. A. Forrest, M. J. Zaworotko, K.-J. Chen, *journal of the American Chemical Society* **2021**, *143*, 1485-1492.

[11] Q. Ding, Z. Zhang, Y. Liu, K. Chai, R. Krishna, S. Zhang, *Angewandte Chemie International Edition* **2022**, *61*, e202208134.

[12] G.-D. Wang, Y.-Z. Li, W.-J. Shi, L. Hou, Y.-Y. Wang, Z. Zhu, *Angewandte Chemie International Edition* **2022**, *61*, e202205427.

[13] Z. Jiang, L. Fan, P. Zhou, T. Xu, S. Hu, J. Chen, D.-L. Chen, Y. He, *Inorganic Chemistry Frontiers* **2021**, *8*, 1243-1252.

[14] L. Fan, P. Zhou, X. Wang, L. Yue, L. Li, Y. He, *Inorganic Chemistry* **2021**, *60*, 10819-10829.

[15] X.-W. Gu, J.-X. Wang, E. Wu, H. Wu, W. Zhou, G. Qian, B. Chen, B. Li, *Journal of the American Chemical Society* **2022**, *144*, 2614-2623.

[16] J. Liu, J. Miao, H. Wang, Y. Gai, J. Li, *AIChE Journal* **2023**, *n/a*, e18021.

[17] Y. Wang, C. Hao, W. Fan, M. Fu, X. Wang, Z. Wang, Y. L. Lei Zhu, X. Lu, F. Dai, Z. Kang, R. Wang, W. Guo, S. Hu, D. Sun, *Angewandte Chemie International Edition* **2021**, *60*, 11350-11358.

[18] Y. Wang, M. Fu, S. Zhou, H. Liu, X. Wang, W. Fan, Z. Liu, Z. Wang, D. Li, H. Hao, X. Lu, S. Hu, D. Sun, *Chem* **2022**, *8*, 3263-3274.

[19] H.-T. Wang, Q. Chen, X. Zhang, Y.-L. Zhao, M.-M. Xu, R.-B. Lin, H. Huang, L.-H. Xie, J.-R. Li, *Journal of Materials Chemistry A* **2022**, *10*, 12497-12502.

[20] Y.-Y. Xiong, C.-X. Chen, T. Pham, Z.-W. Wei, A. Forrest Katherine, M. Pan, C.-Y. Su, *CCS Chemistry* **2023**, *0*, 1-14.
[21] J. Liu, H. Wang, J. Li, *Chemical Science* **2023**, *14*, 5912-5917.
[22] J. Liu, K. Zhou, S. Ullah, J. Miao, H. Wang, T. Thonhauser, J. Li, *Small* **2023**, *19*, 2304460.
[23] H.-M. Wen, C. Yu, M. Liu, C. Lin, B. Zhao, H. Wu, W. Zhou, B. Chen, J. Hu, *Angewandte Chemie International Edition* **2023**, *62*, e202309108.